CAMBRIDGE
UNIVERSITY PRESS

Article

Instalment of the margarosanite group, and data on walstromite–margarosanite solid solutions from the Jakobsberg Mn–Fe deposit, Värmland, Sweden

Dan Holtstam[1] , Fernando Cámara[2] and Andreas Karlsson[1]

[1]Department of Geosciences, Swedish Museum of Natural History, Box 50007, SE-104 05 Stockholm, Sweden; and [2]Università degli Studi di Milano, Dipartimento di Scienze della Terra 'A. Desio', Via Luigi Mangiagalli 34, 20133, Milano, Italy

Abstract

The margarosanite group (now officially confirmed by IMA-CNMNC) consists of triclinic Ca-(Ba, Pb) cyclosilicates with three-membered $[Si_3O_9]^{6-}$ rings (3R), with the general formula $AB_2Si_3O_9$, where A = Pb, Ba and Ca and B = Ca. A closest-packed arrangement of O atoms parallel to (101) hosts Si and B cations in interstitial sites in alternating layers. The 3R layer has three independent Si sites in each ring. Divalent cations occupy three independent sites: Ca in B occupies two nonequivalent sites, $Ca1$ (8-fold coordinated), and $Ca2$ (6-fold coordinated). A (=$Ca3$) is occupied by Pb^{2+} (or Ba^{2+}) in 6+4 coordination, or 6+1 when occupied by Ca; this third site occurs within the 3R-layer in a peripheral position. Three minerals belong to this group: margarosanite (ideally $PbCa_2Si_3O_9$), walstromite ($BaCa_2Si_3O_9$) and breyite ($CaCa_2Si_3O_9$). So far, no solid solutions involving the $Ca1$ and $Ca2$ sites have been described. Therefore, root names depend on the composition of the $Ca3$ site only. Isomorphic replacement at the $Ca3$ sites has been noted. We here report data on a skarn sample from the Jakobsberg Mn–Fe oxide deposit, in Värmland, Sweden, representing intermediate compositions on the walstromite–margarosanite binary, in the range *ca.* 50–70% mol.% $BaCa_2Si_3O_9$. The Pb-rich walstromite is associated closely with celsian, phlogopite, andradite, vesuvianite, diopside and nasonite. A crystal-structure refinement (R_1 = 4.8%) confirmed the structure type, and showed that the $Ca3$ (Ba, Pb) site is split into two positions separated by 0.39 Å, with the Ba atoms found slightly more peripheral to the 3R-layers.

Introduction

Margarosanite, ideally $PbCa_2Si_3O_9$, was first described and named by Ford and Bradley (1916), from the Parker Shaft in the Franklin Zn deposit, New Jersey, USA. Although it is an extremely rare mineral, Flink (1917) shortly thereafter reported its second occurrence, from the Långban Mn–Fe deposit, Värmland County, Sweden. Margarosanite was later also found at the nearby Harstigen and Jakobsberg mines. Anthropogenic margarosanite occurs on corroded lead bullets (Mera *et al.*, 2015). Further studies on Franklin type specimens clarified the crystallography (Armstrong, 1963) and the crystal structure of the mineral (Freed and Peacor, 1969).

Walstromite, $BaCa_2Si_3O_9$, was first described by Alfors *et al.* (1965) from the Big Creek–Rush Creek area, Fresno County, California, USA. It was later reported from several other deposits in Western North America (Dunning *et al.*, 2018) and also from pyrometamorphic rocks (paralavas) of the Hatrurim Formation,

Israel (Krząłała *et al.*, 2020). Dent Glasser and Glasser (1968) determined the crystal structure of synthetic walstromite, confirmed subsequently by Barkley *et al.* (2011) using material from the type locality.

The isostructurality of margarosanite and walstromite was first postulated by Glasser and Glasser (1964) and subsequently confirmed by several authors (Dent Glasser and Glasser, 1968; Freed and Peacor, 1969; Callegari and Boiocchi, 2016; Krząłała *et al.*, 2020).

The Ca equivalent, $CaCa_2Si_3O_9$, has been synthesised under high pressure and characterised (Trojer, 1969). The presence of Ca-silicate phases with margarosanite–walstromite structure type as inclusions in diamonds (Joswig *et al.*, 1999; Stachel *et al.*, 2000; Nasdala *et al.*, 2003; Brenker *et al.*, 2005; Woodland *et al.*, 2020) indicate a potentially Ca-rich lithology in the Earth's deep mantle. The isostructural, high-pressure form of $CaCa_2Si_3O_9$, breyite (Brenker *et al.*, 2021), was discovered as inclusions in a super-deep diamond from the São Luiz placer deposits, Juína, Mato Grosso, Brazil.

The definition of the margarosanite group, presently including the three isostructural members margarosanite, walstromite and breyite, was approved by the Commission on New Minerals, Nomenclature and Classification (CNMNC) of the International

Author for correspondence: Dan Holtstam, Email: dan.holtstam@nrm.se

Mineralogical Association (IMA) in June 2020 (Memorandum 96–SM20, Miyawaki *et al.*, 2020). The proposal to the IMA and the present contribution were instigated by a find of intermediate mineral compositions in the walstromite–margarosanite series, in samples from the Jakobsberg deposit.

Description of walstromite-bearing skarn from the Jakobsberg deposit

The ores of the Jakobsberg deposit (59.83°N, 14.11°E), 1 km southeast of Nordmark, Filipstad, Värmland, Sweden, form separate hausmannite and magnetite–hematite bodies along with characteristic commonly banded skarn masses (Magnusson, 1929). Modest amounts of Mn were mined from here 1864–1918, amounting to an equivalent of ~200 tons of extracted metal (Tegengren, 1924). It is particularly known for exotic mineral assemblages of Pb silicates (Dunn *et al.*, 1985; Charalampides and Lindqvist, 1988; Holtstam and Langhof, 1994) and ferrites (Holtstam, 1994; Holtstam *et al.*, 1995). Jakobsberg belongs to the so-called Långban-type localities (Moore, 1970), carbonate-hosted Fe–Mn–(Ba–Pb–As–Sb) deposits in the Palaeoproterozoic Bergslagen ore region. They occur within supracrustal rock sequences dominated by ~1.9 Ga felsic metavolcanics that altogether have been regionally metamorphosed under mid amphibolite-facies conditions (500–650°C and 200–400 MPa) and to some extent also affected by Svecokarelian intrusive events in the region (Björck, 1986). From a genetic point of view, the Långban-type ore deposits represent metamorphic analogues of shallow-marine, exhalative Mn–Fe deposits (Boström *et al.*, 1979; Holtstam and Mansfeld, 2001).

The sample investigated (GEO-NRM catalogue #19940358) is a medium-grained silicate skarn, with subordinate baryte and native copper present. Carbonates and oxides are absent. The rock is exceedingly heterogeneous in terms of mineral composition, and irregularly banded, as clearly seen under short-wave ultraviolet light. Non-fluorescent parts mainly consist of ganomalite, phlogopite, vesuvianite and andradite. Bright orange-yellow fluorescent wollastonite crystals up to 5 mm occurs with mainly phlogopite and garnet. Minor amounts of ganomalite (low in MnO, ~1 wt.%, thus forming a near-midpoint solid solution with wayneburnhamite, $Pb_9Ca_6(Si_2O_7)_3(SiO_4)_3$; Kampf *et al.*, 2016) are also found here.

A smaller portion of the rock (as 5–15 mm wide bands) is dominated by bluish-white (under ultraviolet) celsian, blue walstromite (i.e. the walstromite–margarosanite solid solution described here), phlogopite and Al-rich andradite. Walstromite forms subhedral, often lamellar crystals up to *ca.* 0.5 mm in longest dimension (Fig. 1), occasionally united in multigranular aggregates, sometimes showing a skeletal to poikiloblastic appearance, with inclusions of celsian. From the textural observations we conclude that phlogopite and celsian are the most primary constituents of the assemblage along with partially resorbed accessory andradite. Fluid-mediated remobilisation of Pb obtained from ganomalite or some other precursor Pb mineral might have led to formation of walstromite–margarosanite. Vesuvianite, Mn-rich diopside and sparse grossular also belong to this association. Nasonite occurs as grains up to 0.3 mm across, usually in direct contact with walstromite. On rims and along cracks and cleavage traces of walstromite, margarosanite with near-end member composition occurs as over- and intergrowths (Fig. 2), interpreted as a late pseudomorphic replacement. As can be seen in back-scatter electron (BSE) images with enhanced contrast, walstromite is sometimes heterogeneous, with a sector-like zonation linked to variations of Ba and Pb contents.

Experimental

Single-crystal X-ray diffraction data were collected with a Rigaku Oxford Diffraction XtaLAB Synergy diffractometer equipped with a PhotonJet (Mo) X-ray Source operating at 50 kV and 1 mA, and a Hybrid Pixel Array detector at 62 mm from the sample position. A large number of images (27,030) were taken at 0.2° rotation of
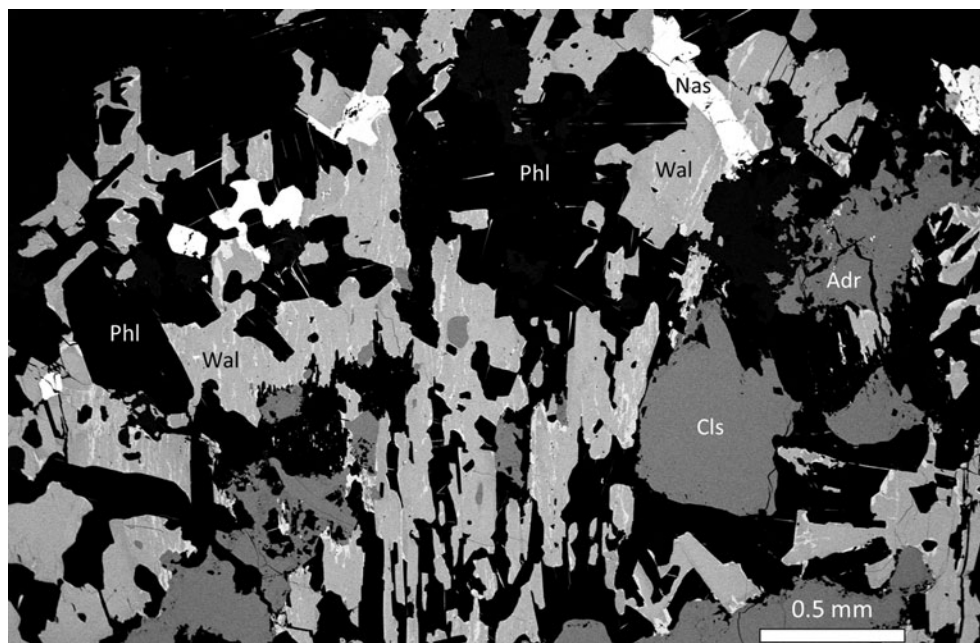
Fig. 1. SEM-BSE image of the mineral assemblage in sample GEO-NRM #19940358, with walstromite–margarosanite (Wal), celsian (Cls), phlogopite (Phl), andradite (Adr) and nasonite (Nas).
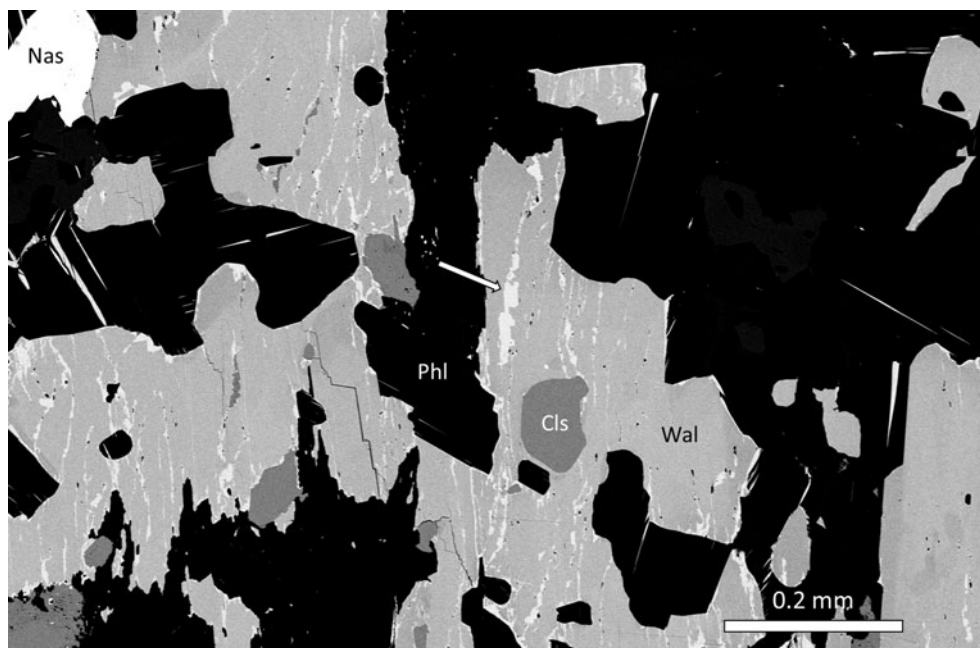
Fig. 2. SEM-BSE image, detail of Fig 1. Arrow points to a phase with margarosanite end-member composition (GEO-NRM catalogue #19940358).

ω-rotations at 0.36 s per exposure in shutterless mode in order to cover a full sphere of the reciprocal space and to get accurate intensity data. The crystal structure was refined using *SHELX-2018* (Sheldrick, 2015), starting from the atomic coordinates of Freed and Peacor (1969). Neutral scattering curves were employed and anisotropic displacement parameters were refined.

Crystal and refinement data are given in Table 1. Atomic coordinates, equivalent displacement parameters, and site occupancies are reported in Table 2, whereas selected bond distances and angles obtained are found in Table 3. The crystallographic information file has been deposited with the Principal Editor of *Mineralogical Magazine* and is available as Supplementary material (see below).

Table 1. Data and experimental details for single-crystal X-ray diffraction study of Pb-rich walstromite from Jakobsberg.

Crystal data	
Ideal formula	$(Ba_{0.57}Pb_{0.43})Ca_2Si_3O_9$
Crystal dimensions (mm)	$0.20 \times 0.15 \times 0.10$
Crystal system, space group	Triclinic, $P\bar{1}$
Temperature (K)	293(2)
a, b, c (Å)	6.73527(7), 9.57172(12), 6.68718(6)
α, β, γ (°)	110.1760(10), 102.6060(8), 83.2059(9)
V (Å^3)	394.466(7)
Z	2
Calculated density (g·cm^{-3})	4.006
μ (mm^{-1})	28.048
Data collection	
Crystal description	Colourless block
Instrument	Rigaku Oxford Diffraction XtaLAB Synergy, HyPix
Radiation type, wavelength (Å)	Mo$K\alpha$, 0.71073 Å
Number of frames	27,030
θ range (°)	2.27 to 45.08
Absorption correction	Multi-scan (*SCALE3 ABSPACK*, Rigaku Oxford Diffraction ®)
T_{min}, T_{max}	0.028, 1
Number of measured, independent and observed reflections	65908, 6531, 5677
R_{int}	0.057
Data completeness to 40.43° (%)	99.9
Indices range of h, k, l	$-13 \leq h \leq 13, -19 \leq k \leq 19, -13 \leq l \leq 13$
Refinement	
Refinement	Full-matrix least-squares on F^2
Number of reflections, parameters, restraints	6531, 147, 0
$R_1 [I > 2\sigma(I)], R_2$ (all)	0.048, 0.0547
GoF	1.25
$wR_1 [I > 2\sigma(I)], wR_2$ (all)	0.105, 0.107
Extinction coefficient	0.0027(5)
$\Delta\rho_{max}, \Delta\rho_{min}$ (e^-Å^{-3})	3.16, −2.14

Table 2. Fractional atomic coordinates, thermal parameters and occupancies.

Site	Atom	x/a	y/b	c/z	U_{eq}
Ca3a*	Ba	0.05053(16)	0.15010(8)	0.31843(17)	0.01179(13)
Ca3b*	Pb	0.08539(15)	0.16033(7)	0.28603(14)	0.01398(12)
Ca1	Ca	0.27312(10)	0.49225(7)	0.76280(10)	0.01143(10)
Ca2	Ca	0.43927(9)	0.17017(7)	0.93833(10)	0.00998(10)
Si1	Si	0.09646(13)	0.77913(10)	0.15456(14)	0.00822(13)
Si2	Si	0.23322(14)	0.51723(10)	0.28343(14)	0.00817(13)
Si3	Si	0.44019(14)	0.80132(10)	0.51420(14)	0.00823(13)
O1	O	0.2317(4)	0.7409(3)	0.9718(4)	0.0115(4)
O2	O	0.1029(4)	0.1240(3)	0.9021(4)	0.0126(4)
O3	O	0.2328(4)	0.8750(3)	0.3927(4)	0.0107(3)
O4	O	0.0451(4)	0.6274(3)	0.1970(4)	0.0108(3)
O5	O	0.3734(4)	0.4423(3)	0.1066(4)	0.0107(3)
O6	O	0.1304(4)	0.4108(3)	0.3636(4)	0.0140(4)
O7	O	0.3600(4)	0.6405(3)	0.5057(4)	0.0115(4)
O8	O	0.4853(4)	0.0943(3)	0.2425(4)	0.0127(4)
O9	O	0.3856(4)	0.2369(3)	0.6289(4)	0.0111(3)

Occupancies: Ca3a = 0.570(4); Ca3b = 0.430(4)

Chemical data were obtained through an FEI Quanta 650 field-emission scanning electron microscope (SEM) fitted with an 80 mm² X-Max^N Oxford Instruments energy-dispersive spectroscopy (EDS) detector (accelerating voltage 20 kV, beam size 1 µm and working distance 10 mm). Beam current was calibrated on Co metal, with the instrument calibrated against reference materials for each element (quartz for Si; wollastonite for Ca, BaF₂ for Ba, PbTe for Pb and pure metal for Mn). Chemical data are available in supplementary material, Table S1.

Micro-Raman measurements were performed using a Horiba (Jobin Yvon) LabRam HR Evolution. Polished sample surfaces were excited with an air-cooled frequency doubled 532 nm Nd-YAG laser utilising an Olympus 100× objective (NA = 0.9). Spectra were generated in the range of 1800 to 200 cm^{-1} utilising a 600 grooves/cm grating. The spectral resolution was in the order of 1 cm^{-1} and the lateral resolution was ~1 µm. The wavenumber calibration was done using the 520.7 cm^{-1} Raman band on a polished Si wafer with a wavenumber accuracy usually better than 0.5 cm^{-1}. The spectra shown (Fig. 3) were collected through two acquisition cycles with single counting times of 45 s in a close to back-scattered geometry, on regions previously analysed during SEM studies.

Mineral chemistry

The sample from the Jakobsberg deposit displays variable Ba–Pb compositions in the range from ca. 50 mol.% margarosanite–50% mol.% walstromite to ca. 30 mol.% margarosanite–70 mol.% walstromite (Fig. 4). The Mn content is low and constant, 0.01–0.02 apfu. No other elements were detected.

Electron probe microanalysis data in the literature show only minor compositional variations for these minerals. Margarosanite from Franklin includes 0.8 wt.% ZnO and 0.6 wt.% MnO (Dunn, 1985), whereas Långban samples could have up to 2.8 wt.% MnO and 0.2 wt.% BaO (Charalampides and Lindqvist, 1988). Walstromite from Fresno, California shows up to 0.4 wt.% SrO, 0.5% wt.% MnO (RRUFF no. R070634.2, Lafuente et al., 2015) and 0.3 wt.% Al₂O₃ (Basciano, 1999), whereas walstromite from Hatrurim contains up to 0.4 wt.% TiO₂ and 0.7 wt.% SrO (Krzątała et al., 2020). Furthermore, there is no evidence for substitution between Ca²⁺ and the two larger cations Ba²⁺ and Pb²⁺ in walstromite or margarosanite, respectively. For breyite, no foreign cations are reported (Brenker et al., 2021). Intermediate compositions between margarosanite and walstromite, indicating an extensive solid-solution series, have never been shown to exist up to now.

Raman spectra

The Raman spectrum of Pb-rich walstromite is affected by both a high fluorescence background (in particular above 800 cm^{-1}) and broadening of peaks (Fig. 3). As expected, there is significant resemblance between the spectra of walstromite and of pure margarosanite (obtained from GEO-NRM #g38818, a Jakobsberg sample). The considerable broadening of the walstromite peaks can be explained by positional disorder induced by randomly distributed Pb/Ba cations; see also Alia et al. (2000).

The prominent Raman band at 654.5 cm^{-1} obtained for end-member margarosanite is related to Si–O–Si symmetric stretching

Table 3. Selected interatomic distances (Å), angles (°), tetrahedral angle variances (TAV, °²) and quadratic elongations (TQE) according to Robinson et al. (1971) for walstromite–margarosanite.

Si1–O1	1.599(4)	Si2–O4	1.684(3)	Si3–O3	1.666(3)		
Si1–O2	1.591(3)	Si2–O5	1.596(3)	Si3–O7	1.670(4)		
Si1–O3	1.666(3)	Si2–O6	1.584(4)	Si3–O8	1.593(3)		
Si1–O4	1.660(4)	Si2–O7	1.675(3)	Si3–O9	1.604(4)		
<Si1–O>	1.6289	<Si2–O>	1.635	<Si3–O>	1.633		
V (Å³)	2.209	V (Å³)	2.220	V (Å³)	2.226		
TQE	1.0033	TQE	1.0073	TQE	1.0035		
TAV (°²)	12.051	TAV (°²)	31.531	TAV (°²)	14.029		
Ca1–O1	2.327(3)	Ca2–O1	2.347(3)	Ca3a–O9	2.702(3)	Ca3b–O9	2.655(3)
Ca1–O4	2.650(4)	Ca2–O2	2.304(3)	Ca3a–O8	3.035(3)	Ca3b–O8	2.748(4)
Ca1–O5	2.444(3)	Ca2–O5	2.484(3)	Ca3a–O6	2.516(3)	Ca3b–O6	2.314(4)
Ca1–O5	2.427(3)	Ca2–O8	2.446(3)	Ca3a–O2	2.805(3)	Ca3b–O2	2.497(4)
Ca1–O6	2.506(3)	Ca2–O8	2.335(4)	Ca3a–O3	2.926(3)	Ca3b–O3	3.057(4)
Ca1–O6	2.811(3)	Ca2–O9	2.313(4)	Ca3a–O4	3.362(4)	Ca3b–O1	2.733(3)
Ca1–O7	2.763(3)	<Ca2–O>	2.372	Ca3a–O1	2.790(3)	Ca3b–O3	3.465(3)
Ca1–O9	2.386(3)	V (Å³)	17.384	Ca3a–O3	3.077(3)	Ca3b–O2	2.891(3)
<Ca1–O>	2.539			Ca3a–O3	2.726(3)	<Ca3b–O>	2.795
V (Å³)	28.040			Ca3a–O7	3.395(3)	V (Å³)	37.069
				<Ca3a–O>	2.933		
				V (Å³)	49.34		
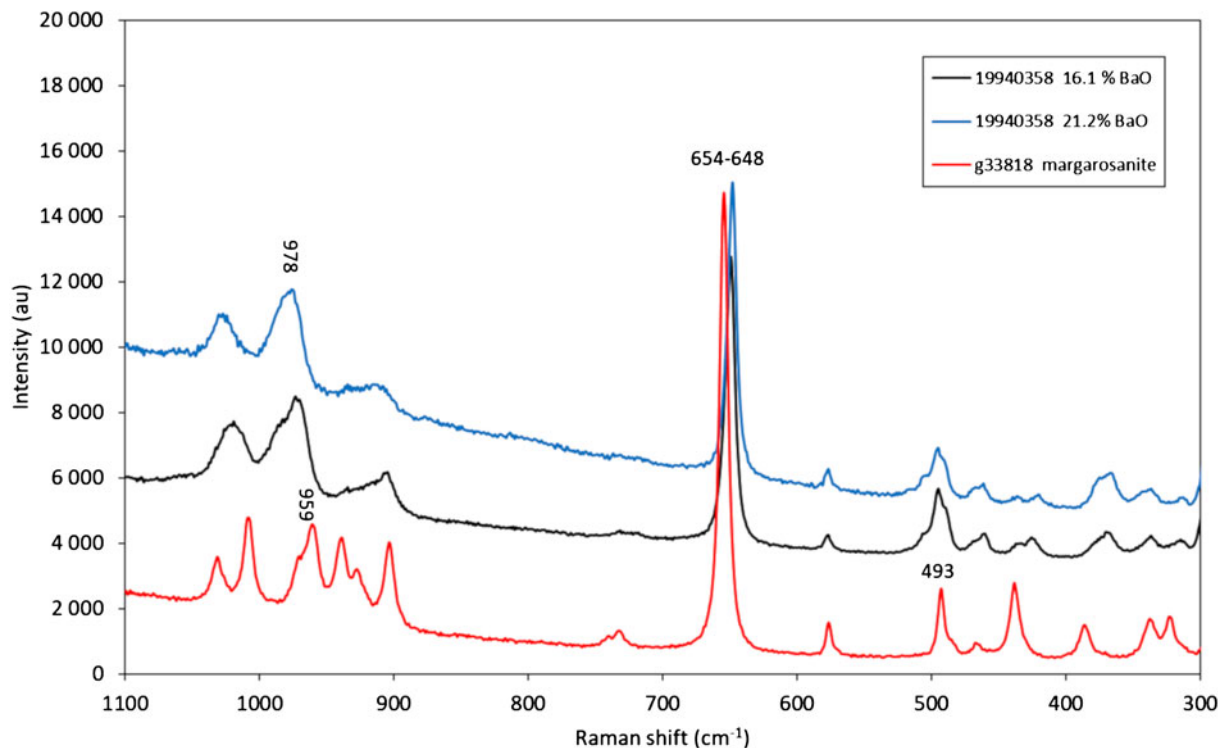
Fig. 3. Raman spectra obtained with a 532-nm laser. Spectra are displaced 4000–6000 units on the Y axis for clarity.
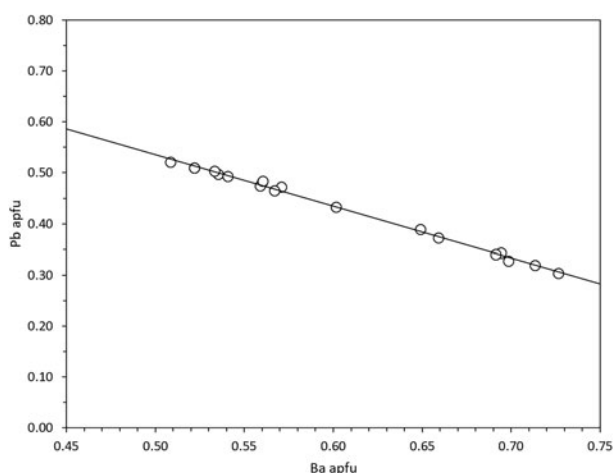
Fig. 4. Chemical variation Ba *vs*. Pb in walstromite–margarosanite based on EDS analyses. The linear regression line ($R^2 = 0.99$) verifies the binary solid solution.

vibrations in the 3-membered silicate rings, analogous to, e.g. the main band at ~580 cm^{-1} of benitoite and isostructural minerals (Takahashi *et al.*, 2008) and the corresponding band at 666 nm in roeblingite (Långban specimen, RRUFF ID: R140328, Lafuente *et al.*, 2015). This particular band is shifted to 650–648 cm^{-1}, and the peak position is sensitive to composition of the analysed spot (shifted to lower frequency with higher BaO contents). The bands at *ca.* 980–960 are possibly related to Si–O stretching vibrations. Distinct bands at *ca.* 576 and 493 cm^{-1} are common for all the spectra and due to bending vibrations in the silicate rings (Chukanov and Chervonnyi, 2016). The intense 1010 cm^{-1} band of pure margarosanite has no defined counterpart in

walstromite. End-member walstromite has a distinct band at 988 cm^{-1} (measured with a 633-nm laser; Gaft *et al.*, 2013), whereas the present analyses of the Jakobsberg sample shows only a broad feature at *ca.* 975 cm^{-1}.

Single-crystal structural study

The minerals of the margarosanite group are Ca-(Ba, Pb) cyclosilicates with three-membered $[Si_3O_9]^{6-}$ rings (3R) in layers with the apices of alternating rings pointing in opposite directions (Fig. 5a,b). The crystal structure can be described as a closest-packing of O atoms with compact layers parallel to (101), hosting Si and Ca (Ba, Pb) cations at interstitial sites. There are three unique Si sites in each ring, whereas Ca occupies two nonequivalent sites: *Ca*1 with 8-coordination to O; and *Ca*2 with 6-coordination. Ba^{2+} and Pb^{2+} reside in a unique 6+4 coordinated position (6+1 for Ca in breyite), within the 3R-layer in a peripheral position.

Trojer (1969) described the structure of 'wollastonite-II' as a high-pressure modification in a synthetic analogue. Later Joswig *et al.* (2003) described 'CaSiO₃-walstromite' and discussed the relationships with 'wollastonite-II'. These authors reported that the axial Si₃O₉-ring could be isomorphously replaced by the same ring with the 'inverse axiality'. A detailed study by Barkley *et al.* (2011) showed that the topology is identical (also to walstromite) and that both structures are equivalent after an opportune transformation of coordinates using the matrix

$$\begin{pmatrix} \bar{1} & \bar{1} & 0 & 1/2 \\ 0 & 1 & 0 & 0 \\ 0 & 0 & \bar{1} & 1/2 \end{pmatrix}$$
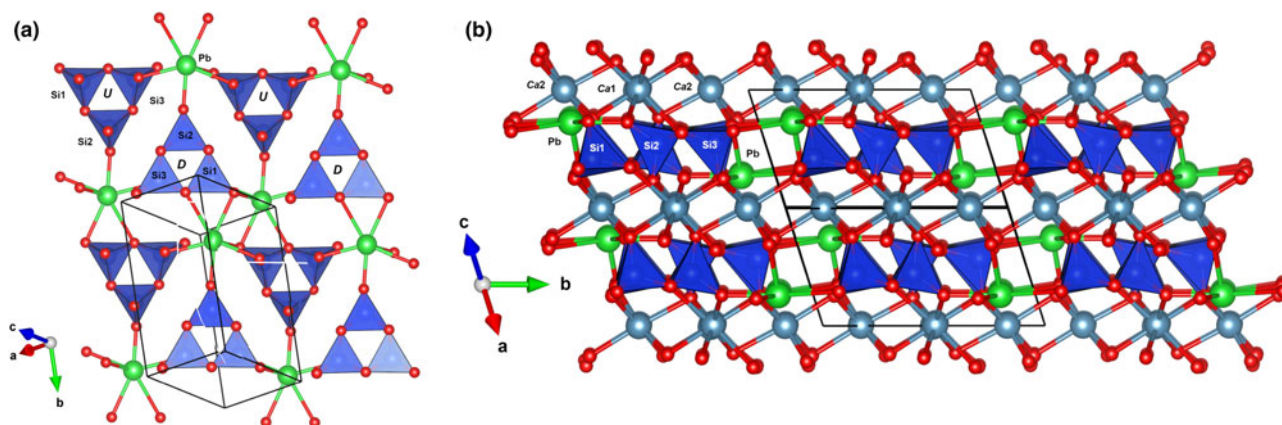
Fig. 5. The 'layer' of 3-membered rings of SiO_4 tetrahedra in margarosanite (a) and the relative position of sites occupied by Ca (Ca1 and Ca2) and by Pb(Ba) (Ca3) (b). Figures obtained with *Vesta 3.0* (Momma and Izumi, 2011).

Table 4. Chemical formulae and crystallographic data for margarosanite-group members (natural samples). Triclinic symmetry, space group $P\bar{1}$ and $Z = 2$.

	Margarosanite[1]	Walstromite[2]	Breyite[3]	Walstromite[4]
Chemical formulae	$PbCa_2Si_3O_9$	$BaCa_2Si_3O_9$	$CaCa_2Si_3O_9$	$(Ba_{0.6}Pb_{0.4})Ca_2Si_3O_9$
Unit-cell parameters				
a (Å)	6.7370(3)	6.7335(2)	6.6970(4)	6.73527(7)
b (Å)	9.5295(4)	9.6142(3)	9.2986(7)	9.57172(12)
c (Å)	6.6961(3)	6.6859(2)	6.6501(4)	6.68718(6)
α (°)	110.185(2)	69.638(2)	83.458(6)	110.1760(10)
β (°)	103.048(2)	102.281(2)	76.226(6)	102.6060(8)
γ (°)	83.037(2)	96.855(2)	69.581(7)	83.2059(9)
V (Å³)	392.63(3)	396.01(2)	376.72(4)	394.466(7)

[1]Callegari *et al.* (2016); [2]Barkley *et al.* (2011); [3]Brenker *et al.* (2021); [4]this work

The corresponding unit-cell parameters for wollastonite-II after the transformation are $a = 6.695$, $b = 9.429$, $c = 6.666$ Å, $\alpha = 83.671$, $\beta = 76.133$ and $\gamma = 67.639°$. This $CaSiO_3$ phase was subsequently thus named breyite (Brenker *et al.*, 2021), also corresponding to the 'walstromite-structured $CaSiO_3$' (e.g. Joswig *et al.*, 1999; Brenker *et al.*, 2007) or '$CaSiO_3$-walstromite' (Barkley *et al.*, 2011; Anzolini *et al.*, 2016).

The unit-cell parameters of all the members of the group, including our new data, are given in Table 4. Whereas those are all isotypic, each mineral has unfortunately been described with a different crystallographic setting. The Niggli cell for margarosanite is: $a = 6.696$, $b = 6.739$, $c = 9.529$ Å, $\alpha = 83.04$, $\beta = 69.81$, $\gamma = 76.95°$ and $V = 392.75$ Å³.

The setting used by Freed and Peacor (1969) can be obtained from the Niggli cell using the matrix

$$\begin{pmatrix} 0 & 1 & 0 \\ 0 & 0 & 1 \\ \bar{1} & 0 & 0 \end{pmatrix}$$

The setting used for walstromite by Dent Glasser and Glasser (1968) can be obtained from the Niggli cell using the matrix

$$\begin{pmatrix} 0 & \bar{1} & 0 \\ 0 & 0 & 1 \\ 1 & 0 & 0 \end{pmatrix}$$

The setting used for breyite by Brenker *et al.* (2021) can be obtained from the Niggli cell using the matrix

$$\begin{pmatrix} 1 & 0 & 0 \\ 0 & 0 & 1 \\ 0 & 1 & 0 \end{pmatrix}$$

The 3R-topology of the rings of SiO_4 tetrahedra is almost unique among minerals. Three-membered rings occur in 'benitoite-group' minerals (benitoite, bazirite and pabstite; informally grouped by Hawthorne, 1987) as well as in wadeite, calciocatapleiite and catapleiite. However, only in the rare complex Pb oxysalt roeblingite, $Pb_2Ca_6(SO_4)_2(OH)_2(H_2O)_4[Mn(Si_3O_9)_2]$, do the SiO_4 tetrahedra have exactly the same configuration as in margarosanite (Moore and Shen, 1984). In margarosanite and roeblingite the tetrahedra in the 3R units point all up or all down (u^3 or d^3, following the Hawthorne *et al.*, 2019 coding for nets) alternating in the same plane containing the 3R-units, whereas in the remaining above mentioned 3R-unit silicates the tetrahedra point neither up nor down (o^3).

The crystal-structure analysis of the Jakobsberg specimen with composition *ca.* $(Ba_{0.57}Pb_{0.43})Ca_2Si_3O_9$ confirmed the structure type. In addition, it can be noted that the Ca3 (Ba, Pb) site is split into two positions separated by 0.392(2) Å, with the position occupied by Ba found slightly more peripheral to the 3R-layers (Fig. 6). Moore *et al.* (1993) compared the crystal structures of end-member margarosanite and walstromite and found a difference of 0.43 Å, ascribed to the stereochemically active $6s^2$ lone
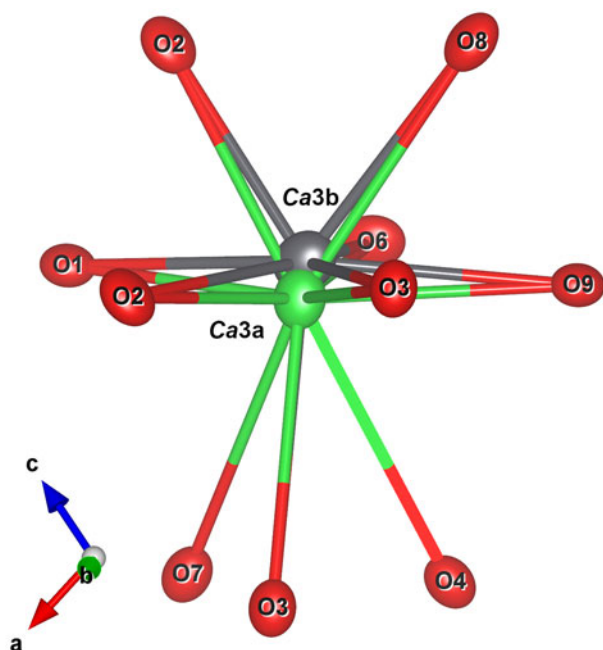
Fig. 6. The *Ca*3 coordination polyhedron with shifted Pb atoms at the *Ca*3b site due to the lone pair effect of Pb^{2+}. Figures obtained with *Vesta 3.0* (Momma and Izumi, 2011).

electron pair of the Pb^{2+} ion. An analogous splitting of ~0.5 Å was found in the structure of hyalotekite $(Ba,Pb,K)_4(Ca,Y)_2(B,Be)_2(Si,B)_2Si_8O_{28}F$, Christy *et al.*, 1998), a mineral described for the first time at Långban (Nordenskiöld, 1877).

Nomenclature

Minerals of the margarosanite group have the general formula $AB_2Si_3O_9$, where *A* (*Ca*3 site) = Ca, Ba and Pb and *B* (*Ca*1 and *Ca*2 sites) = Ca. Root names therefore depend on the composition at *A*. The presence of non-dominant amounts of cations at the *Ca*3 site are described with a modifier (Pb-, Ba- or Ca-rich).

Margarosanite clearly has priority in terms of historical precedence, but the structure type has become more familiar under a different name (walstromite). However, neither the 'margarosanite group' nor the 'walstromite group' seem to have been used as a term used in the past (except for the unapproved use by Krząłała *et al.*, 2020). According to Mills *et al.* (2009), a group name can be selected contrary to the precedence rule when the name of this group is very firmly established in the literature. In this case, we found insufficient arguments to apply this rule of exception.

Further members of the group are possible in Nature. Substitution of Sr for Ca is known in synthetic compounds, such as $Ca_{0.43}Sr_{0.57}[SiO_3]$ (Dörsam *et al.* (2009) and $Sr[SiO_3]$ (Machida *et al.*, 1982), leading to the possible $CaCa_2Si_3O_9$–$SrSr_2Si_3O_9$ solid solution suggested by Barkley *et al.* (2011). A Ba–Sr member seems possible, from the existence of isostructural synthetic $BaSr_2Ge_3O_9$ (Bräuchle *et al.*, 2016). Phosphate structural analogues, e.g. $KNa_2P_3O_9$ (Tordjman *et al.*, 1974) are known as synthetic compounds. If they are discovered in geological environments, a mineral supergroup of the general formula $AB_2T_3O_9$ should be defined. Interestingly, a high-pressure polymorph of Fe-rich dolomite, 'dolomite-IV', has a topologically similar crystal structure (with tetrahedrally coordinated C atoms; Merlini *et al.*, 2017).

Comment on Ba–Pb isomorphism

Ba-for-Pb replacement is very rare among silicate minerals, found only in the hyalotekite group (Hawthorne *et al.*, 2018). Members of the feldspar group could potentially host large amounts of Pb, such as in the Pb-rich orthoclase from Broken Hill, NSW, Australia (e.g. Plimer, 1976). Celsian in the present sample has no Pb (at the EDS detection limit, ≥ 0.2 wt.% PbO). Celsian from Jakobsberg is shown to be dominantly Al–Si ordered, has the monoclinic $I2/c$ structure (Griffin and Ribbe, 1976), and is essentially isostructural with ordered synthetic $PbAl_2Si_2O_8$ (Benna *et al.*, 1996). There is no obvious reason why intermediate $(Pb,Ba)Al_2Si_2O_8$ compositions should not exist in Nature, in the same fashion as for margarosanite–walstromite, provided that the appropriate bulk composition can be achieved. The most Ba–Pb-rich feldspar known is a hyalophane from the Långban deposit (Christy and Gatedal, 2005). The effect of the Pb^{2+} lone pair in feldspar is displacive for the Pb atoms, and it changes the anion coordination from nominally 7-fold to an irregular 6-fold configuration (Benna *et al.*, 1996). Such phenomena could have an effect on the solid solubility, but are largely still unexplored. Margarosanite is stable to ~800°C at ambient pressure (Jak *et al.*, 1998), whereas walstromite has an extended stability to at least 1200°C (Shukla *et al.*, 2018). No data are available for intermediate compositions of the series. If a solvus exists in it, the corresponding immiscibility gap must lie below the maximum temperature of regional metamorphism, not greatly exceeding 650°C in the area.

References

Alfors J.T., Stinson M.C., Matthews R.A. and Pabst A. (1965) Seven new barium minerals from eastern Fresno County, California. *American Mineralogist*, **50**, 314–340.

Alia J.M., Edwards H.G.M., Lopez-Andres S., Gonzalez-Martin P., Garcia-Navarro F.J. and Mansour H.R. (2000) FT-Raman study of three synthetic solid solutions formed by orthorhombic sulfates: celestite-barytes, barytes-anglesite and celestite-anglesite. *Spectroscopy Letters*, **33**, 323–336.

Anzolini C., Angel R.J., Merlini M., Derzsi M., Tokár K., Milani S., Krebs M.Y., Brenker F.E., Nestola F. and Harris J.W. (2016) Depth of formation of CaSiO₃-walstromite included in super-deep diamonds. *Lithos*, **265**, 138–147.

Armstrong R.L. (1963) New data on margarosanite. *American Mineralogist*, **48**, 698–703.

Barkley M.C., Downs R.T. and Yang H. (2011) Structure of walstromite, $BaCa_2Si_3O_9$, and its relationship to $CaSiO_3$-walstromite and wollastonite-II. *American Mineralogist*, **96**, 797–801.

Basciano L.C. (1999) *Mineralogy and Crystal Structures of Barium Silicate Minerals from Fresno County, California*. Doctoral dissertation, University of British Columbia, Canada, 151 pp.

Benna P., Tribaudino, M. and Bruno E. (1996) The structure of ordered and disordered lead feldspar $(PbAl_2Si_2O_8)$. *American Mineralogist*, **81**, 1337–1343.

Björck L. (1986) Beskrivning till berggrundskartan Filipstad NV. *Sveriges Geologiska Undersökning*, Af **147**, 1–110

Boström K., Rydell H. and Joensuu O. (1979) Långban – An exhalative sedimentary deposit? *Economic Geology*, **74**, 1002–1011.

Bräuchle S., Hejny C. and Huppertz H. (2016) Synthesis and structural characterization of BaSr$_2$Ge$_3$O$_9$. *Zeitschrift für Naturforschung B*, **71**, 1225–1232.

Brenker F.E., Vincze L., Vekemans B., Nasdala L., Stachel T., Vollmer C., Kersten M., Somogyi A., Adams F., Joswig W and Harris J.W. (2005) Detection of a Ca-rich lithology in the Earth's deep (>300 km) convecting mantle. *Earth and Planetary Science Letters*, **236**, 579–587.

Brenker F.E., Vollmer C., Vincze L., Vekemans B., Szymanski A., Janssens K., Szaloki I., Nasdala L., Joswig W and Kaminsky F. (2007) Carbonates from the lower part of transition zone or even the lower mantle. *Earth and Planetary Science Letters*, **260**, 1–9.

Brenker F.E., Nestola F., Brenker L., Peruzzo L. and Harris J.W. (2021) Origin, properties, and structure of breyite: The second most abundant mineral inclusion in super-deep diamonds. *American Mineralogist*, **106**, 38–43.

Callegari A.M and Boiocchi M. (2016) Crystal structure refinement of margarosanite PbCa$_2$Si$_3$O$_9$ and relationship with walstromite BaCa$_2$Si$_3$O$_9$. *Neues Jahrbuch für Mineralogie-Abhandlungen*, **193**, 205–213.

Charalampides G. and Lindqvist B. (1988) Ganomalite, margarosanite and molybdophyllite from Långban, south-central Sweden, and synthetic equivalents. *Meddelanden från Stockholms Universitets Geologiska Institution*, **273 IV**, 1–24.

Christy A.G., Grew E.S., Mayo, S.C., Yates, M.G. and Belakovskiy, D.I. (1998) Hyalotekite, (Ba, Pb, K)$_4$(Ca,Y)$_2$Si$_8$(B, Be)$_2$(Si, B)$_2$O$_{28}$F, a tectosilicate related to scapolite; new structure refinement, phase transitions and a short-range ordered 3b superstructure. *Mineralogical Magazine*, **62**, 77–92.

Christy A.G. and Gatedal K. (2005) Extremely Pb-rich rock-forming silicates including a beryllian scapolite and associated minerals in a skarn from Långban, Värmland, Sweden. *Mineralogical Magazine*, **69**, 995–1018.

Chukanov, N.V. and Chervonnyi, A.D. (2016) *Infrared Spectroscopy of Minerals and Related Compounds*. Springer, Dordrecht, The Netherlands.

Dent Glasser L.S. and Glasser F.P. (1968) The crystal structure of walstromite. *American Mineralogist*, **53**, 9–13.

Dörsam G., Liebscher A., Wunder B., Franz G. and Gottschalk M. (2009) Crystal structure refinement of synthetic Ca$_{0.43}$Sr$_{0.57}$[SiO$_3$]–walstromite and walstromite–fluid Ca–Sr distribution at upper-mantle conditions. *European Journal of Mineralogy*, **21**, 705–714.

Dunn P.J. (1985) The lead silicates from Franklin, New Jersey: occurrence and composition. *Mineralogical Magazine*, **49**, 721–727.

Dunn P.J., Peacor D.R., Valley J.W. and Randall C.A. (1985) Ganomalite from Franklin, New Jersey, and Jakobsberg, Sweden: new chemical and crystallographic data. *Mineralogical Magazine*, **49**, 579–582.

Dunning G.E., Walstrom R.E and Lechner W. (2018) Barium silicate mineralogy of the Western Margin, North American Continent, Part 1: Geology, Origin, Paragenesis and Mineral Distribution from Baja California Norte, Mexico, Western Canada and Alaska, USA. *Baymin Journal*, **19**, 1–70.

Flink G. (1917) Einige Neuigkeiten in schwedischer Mineralogie. *Geologiska Föreningens i Stockholm Förhandlingar*, **39**, 426–452.

Ford W.E. and Bradley W.M. (1916) Margarosanite, a new lead-calcium silicate from Franklin, New Jersey. *American Journal of Science*, **248**, 159–162.

Freed R.L. and Peacor D.B. (1969) Determination and refinement of the crystal structure of margarosanite, PbCa$_2$Si$_3$O$_9$. *Zeitschrift für Kristallographie*, **128**, 213–228.

Gaft M., Yeates H. and Nagli L. (2013) Laser-induced time-resolved luminescence of natural margarosanite Pb(Ca, Mn)$_2$Si$_3$O$_9$, swedenborgite NaBe$_4$SbO$_7$ and walstromite BaCa$_2$Si$_3$O$_9$. *European Journal of Mineralogy*, **25**, 71–77.

Glasser F.P. and Glasser L.D. (1964) Additional notes on margarosanite. *American Mineralogist*, **49**, 781–782.

Griffen D.T. and Ribbe P.H. (1976) Refinement of the crystal structure of celsian. *American Mineralogist*, **61**, 414–418.

Hawthorne F.C. (1987) The crystal chemistry of the benitoite group minerals and structural relations in (Si$_3$O$_9$) ring structures. *Neues Jahrbuch für Mineralogie Monatshefte*, **1987**, 16–30.

Hawthorne F.C., Sokolova E., Agakhanov A.A., Pautov L.A., Karpenko V.Y. and Grew, E.S. (2018) Chemographic exploration of the hyalotekite structure-type. *Mineralogical Magazine*, **82**, 929–937.

Hawthorne F.C., Uvarova Y.A. and Sokolova E. (2019) A structure hierarchy for silicate minerals: sheet silicates. *Mineralogical Magazine*, **83**, 3–55.

Holtstam D. (1994) Mineral chemistry and parageneses of magnetoplumbite from the Filipstad district, Sweden. *European journal of Mineralogy*, **6**, 711–724.

Holtstam D. and Langhof J. (1994) Hancockite from Jakobsberg, Filipstad, Sweden: the second world occurrence. *Mineralogical Magazine*, **58**, 172–174.

Holtstam D. and Mansfeld J. (2001) Origin of a carbonate-hosted Fe–Mn–(Ba–As–Pb–Sb–W) deposit of Långban-type in Central Sweden. *Mineralium Deposita*, **36**, 641–657.

Holtstam D., Norrestam R. and Sjödin A. (1995) Plumboferrite: New mineralogical data and atomic arrangement. *American Mineralogist*, **80**, 1065–1072.

Jak E., Hayes P.C. and Liu N. (1998) Experimental study of phase equilibria in the systems PbO$_x$–CaO and PbO$_x$–CaO–SiO$_2$. *Metallurgical and Materials Transactions B*, **29**, 541–553.

Joswig W., Stachel T., Harris J.W., Baur W.H and Brey G.P. (1999) New Ca-silicate inclusions in diamonds – tracers from the lower mantle. *Earth and Planetary Science Letters*, **173**, 1–6.

Joswig W., Paulus E.F., Winkler B and Milman V. (2003) The crystal structure of CaSiO$_3$–walstromite, a special isomorph of wollastonite-II. *Zeitschrift für Kristallographie*, **218**, 811–818.

Kampf A.R., Housley R.M. and Rossman G.R. (2016) Wayneburnhamite, Pb$_9$Ca$_6$(Si$_2$O$_7$)$_3$(SiO$_4$)$_3$, an apatite polysome: The Mn-free analog of ganomalite from Crestmore, California. *American Mineralogist*, **101**, 2423–2429.

Krzątała A., Krüger B., Galuskina I., Vapnik Y and Galuskin E. (2020) Walstromite, BaCa$_2$(Si$_3$O$_9$), from rankinite paralava within gehlenite hornfels of the Hatrurim Basin, Negev Desert, Israel. *Minerals*, **10**, 407.

Lafuente B., Downs R.T., Yang H. and Stone N. (2015) The power of databases: the RRUFF project. Pp 1–30 in: *Highlights in Mineralogical Crystallography* (T. Armbruster and R.M. Danisi, editors). De Gruyter, Berlin, Germany.

Machida K.-I., Adachi G.-Y., Shiokawa J., Shimada M., Koizumi M., Suito K. and Onodera A. (1982) High-pressure synthesis, crystal structures, and luminescence properties of europium(II) metasilicate and europium(II)-activated calcium and strontium metasilicates. *Inorganic Chemistry*, **21**, 1512–1519.

Magnusson N.H. (1929) Nordmarks malmtrakt: geologisk beskrivning. *Sveriges Geologiska Undersökning*, **Ca13**, 1–98.

Mera M.F., Rubio M., Pérez C.A., Galván V. and Germanier A. (2015) SR μXRF and XRD study of the spatial distribution and mineralogical composition of Pb and Sb species in weathering crust of corroded bullets of hunting fields. *Microchemical Journal*, **119**, 114–122.

Merlini M., Cerantola V., Gatta G.D., Gemmi M., Hanfland M., Kupenko I., Lotti P., Müller H. and Zhang L. (2017) Dolomite-IV: Candidate structure for a carbonate in the Earth's lower mantle. *American Mineralogist*, **102**, 1763–1766.

Mills S.J., Hatert F., Nickel E.H. and Ferraris, G. (2009) The standardisation of mineral group hierarchies: application to recent nomenclature proposals. *European Journal of Mineralogy*, **21**, 1073–1080.

Moore P.B. (1970) Mineralogy and chemistry of Långban-type deposits in Bergslagen, Sweden. *The Mineralogical Record*, **1**, 154–172.

Moore P.B. and Shen J. (1984) Roeblingite, Pb$_2$Ca$_6$(SO$_4$)$_2$(OH)$_2$(H$_2$O)$_4$[Mn(Si$_3$O$_9$)$_2$]: its crystal structure and comments on the lone pair effect. *American Mineralogist*, **69**, 1173–1179.

Moore P.B., Davis A.M., Van Derveer D.G. and Gupta P.S. (1993) Joesmithite, a plumbous amphibole revisited and comments on bond valences. *Mineralogy and Petrology*, **48**, 97–113.

Momma K. and Izumi F. (2011) VESTA 3 for three-dimensional visualization of crystal, volumetric and morphology data. *Journal of Applied Crystallography*, **44**, 1272–1276.

Miyawaki R., Hatert F., Pasero M. and Mills S.J. (2020) Newsletter 56. *Mineralogical Magazine*, **84**, 623–627.

Nasdala L., Brenker F.E., Glinnemann J., Hofmeister W., Gasparik T., Harris J.W., Stachel T. and Reese I. (2003) Spectroscopic 2D-tomography: residual pressure and strain around mineral inclusions in diamonds. *European Journal of Mineralogy*, **15**, 931–935.

Nordenskiöld A.E. (1877) Nya mineralier från Långban. *Geologiska Föreningens i Stockholm Förhandlingar*, **3**, 376–384.

Plimer I.R. (1976) A plumbian feldspar pegmatite associated with the Broken Hill orebodies, Australia. *Neues Jahrbuch für Mineralogie Monatshefte*, **6**, 272–288.

Robinson K., Gibbs G.V. and Ribbe P.H. (1971) Quadratic elongation: a quantitative measure of distortion in coordination polyhedra. *Science*, **172**, 567–570.

Sheldrick G.M. (2015) Crystal structure refinement with SHELXL. *Acta Crystallographica*, **C71**, 3–8.

Shukla A., Jung I.H., Decterov S.A. and Pelton A.D. (2018) Thermodynamic evaluation and optimization of the BaO–SiO$_2$ and BaO–CaO–SiO$_2$ systems. *Calphad*, **61**, 140–147.

Stachel T., Harris J.W., Brey G.P and Joswig W. (2000) Kankan diamonds (Guinea) II: lower mantle inclusion parageneses. *Contributions to Mineralogy and Petrology*, **140**, 16–27.

Takahashi Y., Iwasaki K., Masai H. and Fujiwara T. (2008) Raman spectroscopic study of benitoite-type compounds. *Journal of the Ceramic Society of Japan*, **116**, 1139–1142.

Tegengren F.R. (1924) *Sveriges ädlare malmer och bergverk*. Norstedt, Stockholm.

Tordjman I., Durif A and Cavero-Ghersi B. (1974) Structure cristalline du trimétaphosphate de sodium–potassium: Na$_2$KP$_3$O$_9$. *Acta Crystallographica*, **B30**, 2701–2704.

Trojer F.J. (1969) The crystal structure of a high-pressure polymorph of CaSiO$_3$. *Zeitschrift für Kristallographie*, **130**, 185–206.

Woodland A.B., Girnis A.V., Bulatov V.K., Brey G.P. and Höfer H.E. (2020) Breyite inclusions in diamond: experimental evidence for possible dual origin. *European Journal of Mineralogy*, **32**, 171–185.